A multiscale model for integrating hyporheic exchange from ripples to meanders

Susa H. Stonedahl,[1] Judson W. Harvey,[2] Anders Wörman,[3] Mashfiqus Salehin,[4] and Aaron I. Packman[1]

Received 8 November 2009; revised 21 September 2010; accepted 28 September 2010; published 15 December 2010.

[1] It is necessary to improve our understanding of the exchange of dissolved constituents between surface and subsurface waters in river systems in order to better evaluate the fate of water-borne contaminants and nutrients and their effects on water quality and aquatic ecosystems. Here we present a model that can predict hyporheic exchange at the bed-form-to-reach scale using readily measurable system characteristics. The objective of this effort was to compare subsurface flow induced at scales ranging from very small scale bed forms up to much larger planform geomorphic features such as meanders. In order to compare exchange consistently over this range of scales, we employed a spectral scaling approach as the basis for a generalized analysis of topography-induced stream-subsurface exchange. The spectral model involves a first-order approximation for local flow-boundary interactions but is fully three-dimensional and includes the lateral hyporheic zone in addition to the flow directly beneath the streambed. The primary model input parameters are stream velocity and slope, sediment permeability and porosity, and detailed measurements of the stream channel topography. The primary outputs are the distribution of water flux across the stream channel boundary, the resulting pore water flow paths, and the subsurface residence time distribution. We tested the bed-form-exchange component of the model using a highly detailed two-dimensional data set for exchange with ripples and dunes and then applied the model to a three-dimensional meandering stream in a laboratory flume. Having spatially explicit information allowed us to evaluate the contributions of both gravitational and current-driven hyporheic flow through various classes of stream channel features including ripples, dunes, bars, and meanders. The model simulations indicate that all scales of topography between ripples and meanders have a significant effect on pore water flow fields and residence time distributions. Furthermore, complex interactions across the spectrum of topographic features play an important role in controlling the net interfacial flux and spatial distribution of hyporheic exchange. For example, shallow exchange induced by current-driven interactions with small bed forms dominates the interfacial flux, but local pore water flows are modified significantly by larger-scale surface-groundwater interactions. As a result, simplified representations of the stream topography do not adequately characterize patterns and rates of hyporheic exchange.

Citation: Stonedahl, S. H., J. W. Harvey, A. Wörman, M. Salehin, and A. I. Packman (2010), A multiscale model for integrating hyporheic exchange from ripples to meanders, *Water Resour. Res.*, *46*, W12539, doi:10.1029/2009WR008865.

1. Introduction

[2] Modeling solute transport in streams is critical to evaluating the transport of contaminants, nutrients, and other water-borne constituents, and thus is inherent to the study of ecosystems and water quality. There is a constant exchange of water between streams and the subsurface, generally called hyporheic exchange [*Williams and Hynes*, 1974; *Bencala and Walters*, 1983; *Jones and Mulholland*, 2000]. Stream-borne substances are carried with the water into the subsurface, reside there for some time, and then return to the stream [*Winter et al.*, 1998; *Harvey and Wagner*, 2000; *Packman and Bencala*, 2000]. These stream-subsurface interactions have been demonstrated to control the downstream transport of metals, radionuclides, and arsenic, as well as the release of these substances from contaminated sediments [*Benner et al.*, 1995; *Fuller and Harvey*, 2000; *McKnight et al.*, 2001; *Medina et al.*, 2002]. Hyporheic exchange also has a substantial impact on stream ecology, because it influences

[1]Department of Civil and Environmental Engineering, Northwestern University, Evanston, Illinois, USA.
[2]U.S. Geological Survey, Reston, Virginia, USA.
[3]Royal Institute of Technology, Stockholm, Sweden.
[4]Institute of Water and Flood Management, Bangladesh University of Engineering and Technology, Dhaka, Bangladesh.

0043-1397/10/2009WR008865

nutrient availability and microbial processing of organic matter [*Stream Solute Workshop*, 1990; *Triska et al.*, 1993; *Valett et al.*, 1996; *Mulholland et al.*, 1997; *Jones and Mulholland*, 2000].

[3] Hyporheic exchange results from pressure gradients over the stream channel boundary, which occur over a wide range of scales of topography including meanders, pool-riffle sequences, bars, and bed forms [*Tonina and Buffington*, 2009; *Buffington and Tonina*, 2009; *Cardenas*, 2008; *Wörman et al.*, 2007]. Many studies have focused on the exchange associated with individual features, such as advective flow induced by streamflow over submerged bed forms [*Elliott and Brooks*, 1997a, 1997b; *Cardenas and Wilson*, 2007; *Thibodeaux and Boyle*, 1987] or, on a larger scale, flow induced by elevation gradients around stream meanders [*Cardenas*, 2009a; *Boano et al.*, 2006; *Harvey and Bencala*, 1993]. The topographic spectrum of stream channel morphology normally shows fractal scaling [*Wörman et al.*, 2007; *Nikora et al.*, 1997; *Jerolmack and Mohrig*, 2005], and should be expected to produce complex patterns of hyporheic exchange [*Wörman et al.*, 2007; *Cardenas*, 2008]. However, these multiscale interactions are not currently well understood.

[4] Available models for hyporheic exchange have generally focused on either the use of lumped empirical exchange coefficients to describe solute transport observed in the field, or fundamental modeling of isolated exchange processes under simplified laboratory conditions [*Packman and Bencala*, 2000; *O'Connor and Harvey*, 2008; *Cardenas*, 2008]. Recently, several new process-physics-based models have been developed to describe pore water flows and associated hyporheic exchange that are induced by particular morphological features and scales of stream topography [*Elliott and Brooks*, 1997a; *Packman and Brooks*, 2001; *Cardenas*, 2009a; *Boano et al.*, 2009]. These prior studies suggest that local scale exchange and pore water flow are best simulated using detailed computational fluid dynamics (CFD) models, but alternative approaches are necessary for large systems with complex boundary shapes because it is difficult and time consuming, if not impossible, to apply CFD models for the wide range of scales commonly encountered in fluvial systems. Further, it has also recently been recognized that it is not possible to reduce the hyporheic exchange problem to a summation of independent analyses of numerous individual processes owing to the potential for strong interactions between flows induced at different scales [*Wörman et al.*, 2007; *Cardenas*, 2009b].

[5] Here we provide an approximate approach suitable for assessing interactions of exchange flows across scales. We present a new three-dimensional model for topography-induced exchange in river systems based on an approximate solution obtained using a spectral scaling approach [*Wörman et al.*, 2006]. The model is intended to be applicable to low-gradient (<5%) systems with gradually varied flow, as occurs in most of the small agricultural streams in the United States. The model predicts hyporheic exchange in three dimensions at the bed-form-to-reach scale based on readily measurable system characteristics, such as channel planform morphology, bed morphology, sediment permeability, and average streamflow conditions. The primary advantage of this approximate method is that it represents three dimensional patterns of exchange associated with multiple scales of fluvial topography spanning ripples, dunes, alternate bars, and meanders, as illustrated in Figure 1.

2. Modeling Approach

[6] Our approach to modeling surface-subsurface interactions involves three essential steps: calculating the head distribution on the stream channel boundary, calculating the subsurface flow field, and evaluating the resulting interfacial fluxes, subsurface flow paths and residence time distributions. A brief overview of the approach is provided here, and details follow in sections 2.1–2.3. The estimation of the head distribution along the entire stream bottom and submerged portion of the banks is critical to the calculation of hyporheic fluxes and residence times. This calculation is challenging because of the very wide variety of topographical features that induce interfacial and pore water flows. In particular, a key challenge here was to estimate the boundary head distribution along the stream channel without using CFD simulations, which are generally not feasible for large, multiscale problems. We developed a model that includes gravitational head gradients associated with downstream elevation changes and an approximate solution for velocity head gradients induced by the interaction of the streamflow with the channel boundary. The gravitational component was obtained directly from the average gradient of the stream over the study reach, obtained from water elevation measurements, and then head fluctuations due to smaller topographical features within the stream channel were superimposed. We approximated the head variation over submerged bed forms by generalizing an available two-dimensional solution for advective pore water flow under dunes [*Elliott and Brooks*, 1997a]. We implemented this solution in 3-D by employing a Schwarz-Christoffel conformal mapping procedure [*Zarrati et al.*, 2005] to create a nonorthogonal coordinate system following the curving stream channel. This method provides consistent results regardless of the orientation of the stream, and was used to evaluate the effects of the gravitational head gradient on the three-dimensional stream topography as well as the distribution of velocity head associated with submerged topographic features within the meandering channel. Effectively, the generalized flow-boundary interaction model calculates the pressure distribution over bed forms relative to the direction and magnitude of the local stream velocity. The interfacial head distribution over the stream channel boundary was obtained simply as the sum of the gravitational and velocity head components. This head distribution was then employed as a boundary condition in a finite difference solution for subsurface water flow, allowing lateral (floodplain) exchange and broader stream-groundwater interactions to be simulated along with the local exchange associated with bed forms. The resulting subsurface flow field was then used to evaluate interfacial fluxes by integrating the local pore water velocity over the bed surface. Hyporheic exchange flow paths and residence time distributions were also obtained directly from the subsurface flow field by means of a numerical particle tracking method.

2.1. Representation of Channel Topography

2.1.1. Conformal Mapping

[7] The morphology of the meandering channel was transformed into an orthogonal domain using Schwarz-Christoffel

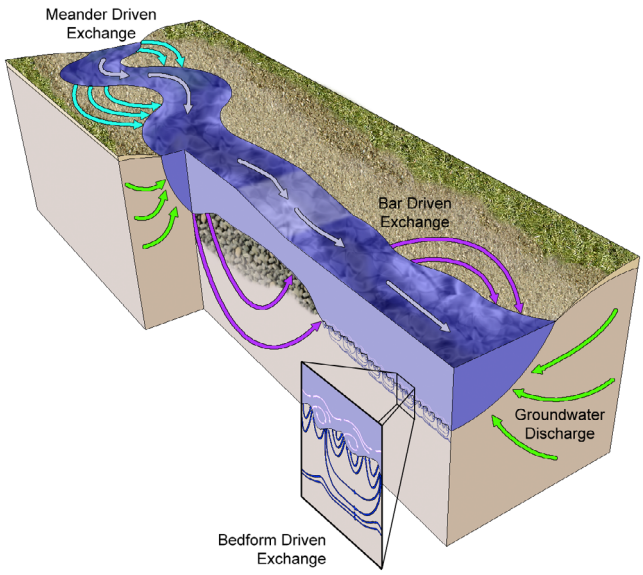

Figure 1. Hyporheic exchange associated with ripples, dunes, bars, and meanders. Reach-scale patterns of exchange reflect complex interactions between these features and larger-scale groundwater discharge/recharge.

conformal mapping. Conformal mapping preserves local angles while producing a one-to-one mapping between differently shaped domains. A polygonal representation of the meandering stream was mapped onto a rectangle using the SC-Toolbox for MATLAB [*Driscoll*, 1996]. This mapping onto a rectangle was found by combining the solution for a bi-infinite strip with a Jacobi elliptic function. The calculation used a Gauss-Newton method for numerically solving a system of nonlinear equations. The conformal mapping is illustrated in Figure 2. The longitudinal and transverse coordinates are defined as x and y, while in the transformed domain these are ξ and η, respectively.

[8] The channel banks were calculated by selecting the grid points closest to where the stream water surface intersected the three dimensional topography grid. The banks were used to define a polygon, which was formatted into complex coordinates with the vertices listed counterclockwise. This polygon was then transformed into a rectangle using Driscoll's algorithm. Characterization of the system geometry was facilitated by the conformal mapping. We calculated length of the stream by taking the inverse mapping of 1000 evenly spaced points along the centerline of the rectangle in the transformed domain. The sum of the distances between these corresponding points (x, y) in the stream provides a good approximation of the length of the stream

$$S = \sum_{i=1}^{N-1} \sqrt{(x_i - x_{i+1})^2 + (y_i - y_{i+1})^2} = \sum_{i=1}^{N-1} \Delta\xi, \qquad (1)$$

where N is the number of points. The sinuosity of the channel was then determined as the ratio of the stream length to the reach length. The width of the stream at each cross section was found similarly to the length. For this calculation, we took the inverse conformal mapping of points along each cross section in the transformed domain and summed the distances between them in the real domain. These values were then averaged to find the mean width of the system. The average depth and cross-sectional areas were also calculated similarly using the elevations at each cross section in the real domain. Discharge was assumed to be constant throughout the reach, and the cross-sectional areas were used to determine how the mean velocity varied as a function of downstream distance.

2.1.2. Fourier Fitting

[9] A Fourier fitting procedure was used for several purposes in the model: (1) to generate a continuous function for topography in both the real and transformed domains, (2) as a means of separating different scales of topography by wavelength in the Fourier series, and (3) as a means of calculating the boundary head distribution from the topographic distribution and streamflow conditions. A trigonometric polynomial finite Fourier series, $P(x, y)$, having the form given in equation (2) was used to represent topography. The coefficients were calculated in MATLAB using a three-dimensional extension of the trigonometric polynomial approximation method [*Fink and Mathews*, 1999, chap. 5]

$$\begin{aligned} P(x,y) = \frac{a_o}{2} + \sum_{j_x=1}^{M_x}\sum_{j_y=1}^{M_y} \big(a_{j_x j_y}\cos(j_x k_x x)\cos(j_y k_y y) \\ + b_{j_x j_y}\sin(j_x k_x x)\cos(j_y k_y y) + \ldots c_{j_x j_y}\cos(j_x k_x x)\sin(j_y k_y y) \\ + d_{j_x j_y}\sin(j_x k_x x)\sin(j_y k_y y)\big) + \sum_{j_x=1}^{M_x}\big(e_j\cos(j_x k_x x) \\ + f_j\sin(j_x k_x x)\big) + \ldots \sum_{j_y=1}^{M_y}\big(g_j\cos(j_y k_y y) + h_j\sin(j_y k_y y)\big). \end{aligned} \qquad (2)$$

The angular wave number for each of the terms was the product of an integer and the wave number, k_x or k_y, where $k_x = 2\pi/\lambda_x$ and $k_y = 2\pi/\lambda_y$. λ_x is both the maximum wavelength and size of the domain in the longitudinal direction and λ_y is the maximum wavelength and size of the domain in the transverse direction. In equation (2), the wavelength of each term is an integer fraction of the maximum wavelength. By imposing these restrictions on the selection of the angular wave numbers used in the Fourier series, each of the resulting wavelengths divides evenly into the domain size, causing the function to be periodic in both the longitudinal and transverse directions. This periodicity is essential for the calculation of head variation over small bed form topography (ripples and dunes), which would otherwise generate unrealistic topography outside of the computational domain [*Wörman et al.*, 2006]. This condition also made it important to start and end the reach at similar locations rela-

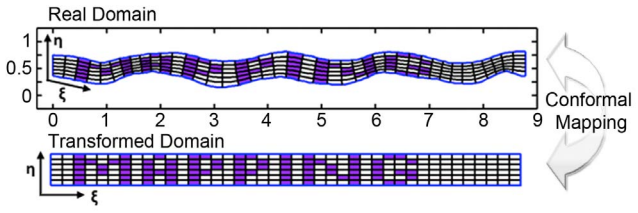

Figure 2. Illustration of Schwarz-Christoffel conformal mapping used to transform the meandering stream with (x, y) coordinates into a rectangle with ($\xi.\eta$) coordinates.

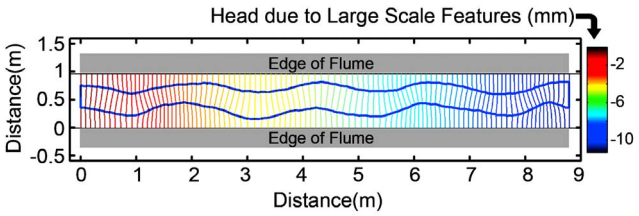

Figure 3. Gravitational head due to large-scale features is held constant for each cross section by applying it in the transformed coordinate system. Within the stream this shows cross sections with uniform gravitational head values, which are roughly perpendicular to the banks. Outside of the stream channel the head contours straighten back out and are perpendicular to the flume walls by the time the edges are reached.

tive to the larger-scale channel topography, here the apexes of two meanders. In real systems, the topography outside of the study reach is generally unknown, so it is reasonable to assume periodicity in the topography before and after the study reach. However, this assumption may be inappropriate if stream characteristics show distinct trends in the longitudinal direction.

[10] The accuracy of the fitting procedure depends on the number of wavelengths used to fit the surface in each direction, M_x and M_y. Each additional wavelength improves the accuracy of the Fourier fit, but only up to the maximum accuracy set by the spatial resolution and quality of the original topographic data. We set M_x and M_y to be one less than half of the number of data points in each direction to comply with the Nyquist frequency cutoff, corresponding to the maximum information content of the data set. Using frequencies greater than the Nyquist cutoff does not provide any additional information and instead induces extraneous fluctuations in the surface, which would yield spurious pore water flows. Unlike previous work [*Wörman et al.*, 2006], which used a limited number of terms in the Fourier series used to represent the surface topography, we used all terms up to the Nyquist frequency cutoff, which used the maximum information content of the data sets.

2.2. Calculation of the Boundary Head Distribution

[11] It is necessary to calculate the head distribution over large and small topographic features separately because flow-boundary interactions produce substantial head gradients over steep features such as dunes, but not over larger and smoother features such as meanders. In general, there is a variation of velocity head over any submerged shape, but particularly large pressure gradients are produced wherever there is a flow separation and recirculation. This occurs primarily at bed form crests [*Thibodeaux and Boyle*, 1987; *Elliott and Brooks*, 1997a; *Cardenas et al.*, 2008; *Cardenas*, 2008]. Thus, local variations in velocity head over bed forms represent important local perturbations to the energy grade line of the stream. We used an approximate criterion to separate the bed topography into two classes of features: large topography for which only the mean energy grade line is used to calculate the boundary head distribution, and small topography for which local variability in velocity head is included in the boundary head distribution. We established the cutoff threshold based on the range of applicability of the gradually varied flow equations. In order for the large-scale topography to comply with the gradually varied flow equations, the slope must be less than 5% [*Chaudhry*, 1993], so the threshold wavelength, λ_c, was chosen such that all features identified as large topography have slope no greater than 5%. This scale separation provides a further advantage in that it also prevents the generation of spurious head fluctuations over large morphological features with amplitudes exceeding the mean flow depth, but over very long wavelengths. The procedures for calculating the boundary head distribution over each of these scales of topographical features are detailed below.

2.2.1. Head Distribution Over Large-Scale Topography

[12] The head distribution over large-scale topographic features ($\lambda > \lambda_c$) was obtained from the energy grade line over the reach. It is difficult to measure the elevation of the free surface precisely, which leads to large errors in the estimation of the hydraulic gradient over small separation distances. Even for the relatively high-density laboratory data sets used here for the initial model application, we found that the free surface measurements were only sufficient to enable estimation of the mean longitudinal hydraulic slope of the flume. The constant slope was applied in the transformed domain, which is equivalent to applying head values corresponding to the slope to each cross section in the real domain. To illustrate the results of this process, Figure 3 shows gravitational head contours within the stream boundary for one of our data sets. (The method for calculating the head contours outside of the stream boundaries is discussed in section 2.3.) Specifically, Figure 3 illustrates how the linear gradient in the transformed domain follows the stream channel in the real domain.

2.2.2. Small-Scale Topography Head Distribution

[13] Streamflow over small-scale topographic features produces regular perturbations in the boundary head distribution that generate important components of the subsurface flow [*Thibodeaux and Boyle*, 1987; *Elliott and Brooks*, 1997a; *Cardenas*, 2008]. The velocity head perturbation over a ripple- or dune-shaped feature is known to be approximately sinusoidal [*Elliott and Brooks*, 1997a, 1997b]. We generalized this solution in two dimensions by representing the boundary head distribution, $h_1(x)$, as a sine curve with a scaled amplitude shifted a quarter of a wavelength from the topography function, $t_1(x)$,

$$t_1(x) = \frac{H}{2}\sin(kx), \tag{3}$$

$$h_1(x) = h_m \sin k\left(x + \frac{\lambda}{4}\right), \tag{4}$$

where h_m is the amplitude of the head distribution, H is the bed form height, k is the wave number, λ is the wavelength, and x is the longitudinal direction. Using this approach, the boundary head distribution is obtained as a Fourier series, where each term is obtained directly from the Fourier series used to represent the streambed topography. *Fehlman*'s [1985] correlation was used to estimate the amplitude of the dynamic head variation for each term

$$h_m = 0.28\left(\frac{V^2}{2g}\right)\begin{cases}\left(\dfrac{H/d}{0.34}\right)^{3/8} & H/d \le 0.34\\ \left(\dfrac{H/d}{0.34}\right)^{3/2} & H/d \ge 0.34\end{cases}, \tag{5}$$

where h_m is the amplitude of the head perturbation, V is the mean velocity of the overlying flow, d is the mean flow depth, and g is the gravitational constant. This equation has been shown to work well as an estimator of pore water flow paths and surface-subsurface exchange under two-dimensional bed forms, i.e., regular dunes that span the width of the flow [*Elliott and Brooks*, 1997a], and is extended here to three-dimensional features. The conformal mapping described above ensures that the sinusoidal head profile is aligned with the direction of the local stream velocity, which varies throughout a three-dimensional stream channel. In the transformed domain, we Fourier fit a scaled version of the topography and calculated the velocity head by shifting each component of the Fourier series by one quarter of its wavelength in the negative ξ direction, following equation (4). This creates an approximate three-dimensional solution for the boundary head distribution with a region of higher head on the upstream side of each bed form. This model is quasi-three-dimensional because we generalized the 2-D solution (equations (3)–(5)) relative to the local channel planform morphology following the longitudinal conformal lines. We expect this approximation to be reasonable given the strongly two-dimensional nature of river flows and dune morphology; however, cases with a high degree of cross-channel variability and/or strongly three-dimensional bed forms may not be represented well.

[14] Stream velocities, depths, and bed form sizes can be highly variable such that mean values for the entire reach may not accurately represent the characteristics of a smaller channel segment. From equation (5), it can be seen that fluctuations in the stream depth and velocity associated with slowly varying large-scale topography affect the estimate of exchange resulting from local scale flow-boundary interactions. In addition, bed form morphology often varies significantly within a reach. To account for this variability, we calculated continuous functions of d, V, and H to scale the velocity head component of the boundary head distribution at each point of the stream. The local stream depth $d(\xi)$ was first calculated as a moving average of the average depth for each cross section over a window size λ_c centered at ξ. The elevation perturbation specifically associated with bed forms, $\varepsilon(\xi)$, was then calculated by subtracting $d(\xi)$ from the average depth for each cross section. In previous work, H has been found from the standard deviation of local bed elevation measurements, σ_H. Specifically, *Elliott and Brooks* [1997a, 1997b] used $H = 2\sigma_H$ as an approximate average bed form height for exchange with a regular series of 2-D dunes. Here, we obtained $\sigma_H(\xi)$ by taking the standard deviation of points in $\varepsilon(\xi)$ over a window size λ_c centered at ξ. This extends the model to include slowly varying channel morphology. For a perfectly sinusoidal topography, $\sigma = \sqrt{\int_0^{2\pi} \left((H/2)\sin(x)\text{^}2\right)/2\pi} = H/2\sqrt{2}$, yielding $2\sqrt{2}\ \sigma = H$. Further, for the triangular bed forms used by Elliott as test cases [*Elliott and Brooks*, 1997b], taking $H = 2\sqrt{2}\sigma$ matches the measured heights of individual dunes within 3%. Therefore we evaluated the bed form height used in equation (5) as $2\sqrt{2}\sigma_H(\xi)$. The average stream velocity, $V(\xi, \eta)$, varies in both the longitudinal and transverse directions. The mean velocity for each cross section is simply the volumetric water flux. This was calculated in the model by dividing the discharge (which was constant) by the local cross-sectional area (which varied). We included a simple first-order correction to account for the transverse velocity profile within each cross section by assuming that V is proportional to depth. This caused the maximum velocity to occur in the thalweg and forced V = 0 at the edges of the channel, which was required to provide a realistic representation of lateral exchange through the stream banks. This transverse variation in the stream velocity created greater fluctuations in velocity head in the deeper portions of the channel relative to the surrounding shallow areas, leading to transverse pore water velocity components.

[15] The final scaling function for the velocity head perturbation over small topography (bed forms) including spatial variability in velocity, depth, and amplitude is

$$h'_m(\xi,\eta) = \frac{0.28\left(\frac{V(\xi,\eta)^2}{2g}\right)}{\sqrt{2}\sigma_H(\xi)} \times \begin{cases} \left(\frac{2\sqrt{2}\sigma_H(\xi)/d(\xi)}{0.34}\right)^{3/8} & 2\sqrt{2}\sigma_H(\xi)/d(\xi) \le 0.34 \\ \left(\frac{2\sqrt{2}\sigma_H(\xi)/d(\xi)}{0.34}\right)^{3/2} & 2\sqrt{2}\sigma_H(\xi)/d(\xi) \ge 0.34 \end{cases}. \tag{6}$$

After the topography is multiplied by $h'_m(\xi, \eta)$, the resulting Fourier series for the distribution of velocity head over the stream channel resulting from flow-boundary interactions in the transformed domain is

$$\begin{aligned} F_h(\xi,\eta) = \frac{A_o}{2} + \sum_{j_\xi=1}^{M_\xi}\sum_{j_\eta=1}^{M_\eta}\Bigg(& A_{j_\xi j_\eta}\cos\left(j_\xi k_\xi \xi + \frac{2\pi}{4j_\xi k_\xi}\right)\cos\left(j_\eta k_\eta \eta\right) \\ & + B_{j_\xi j_\eta}\sin\left(j_\xi k_\xi \xi + \frac{2\pi}{4j_\xi k_\xi}\right)\cos\left(j_\eta k_\eta \eta\right) \\ & + \ldots C_{j_\xi j_\eta}\cos\left(j_\xi k_\xi \xi + \frac{2\pi}{4j_\xi k_\xi}\right)\sin\left(j_\eta k_\eta \eta\right) \\ & + D_{j_\xi j_\eta}\sin\left(j_\xi k_\xi \xi + \frac{2\pi}{4j_\xi k_\xi}\right)\sin\left(j_\eta k_\eta \eta\right)\Bigg) \\ & + \ldots \sum_{j_\xi=1}^{M_\xi}\left(E_j\cos\left(j_\xi k_\xi \xi + \frac{2\pi}{4j_\xi k_\xi}\right)\right. \\ & \left. + F_j\sin\left(j_\xi k_\xi \xi + \frac{2\pi}{4j_\xi k_\xi}\right)\right) \\ & + \sum_{j_\eta=1}^{M_\eta}\left(G_j\cos\left(j_\eta k_\eta y\right) + H_j\sin\left(j_\eta k_\eta \eta\right)\right), \end{aligned} \tag{7}$$

where k_ξ and k_η are the wave numbers corresponding to the maximum wavelength in each direction of the conformal domain, A, B, C, … H are the amplitudes of the Fourier series, and M_ξ and M_η are the number of terms used in each direction. The total head distribution over the stream channel boundary in the real domain, $h(x, y)$, is obtained as the sum of the velocity head fluctuation induced by streamflow over small channel topography, obtained by the inverse conformal mapping of equation (7), and the gravitational head component associated with the slope of the stream.

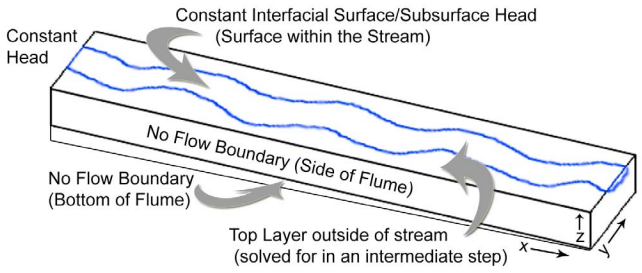

Figure 4. Boundary conditions of the modeling domain for the finite difference calculation. The bottom and walls of the flume are no flow boundaries. The upstream and downstream boundaries are constant heads given by the values of the head in the surface layer. The surface layer is found during an intermediate two-dimensional calculation and is held constant for the three-dimensional calculation.

2.3. Three-Dimensional Simulation of Subsurface Flow

[16] MODFLOW [*Harbaugh et al.*, 2000] was used to calculate the three-dimensional distribution of head and velocity in the subsurface. For the initial application to flume experiments, the entire sedimentary system was included in the computational domain, as shown in Figure 4. The upstream and downstream boundaries were defined as constant heads, which were set in the flume by the selected discharge, the flume geometry, and hydraulic controls at the inlet and outlet. The flume bottom and walls defined no-flow boundaries. The surface-subsurface interface was used as a constant head boundary after the boundary head distribution was calculated as described in section 2.2. In the three-dimensional case additional steps were required to calculate the free surface outside of the stream channel.

[17] Pore fluid flow was calculated from the three-dimensional subsurface head distribution using Darcy's law, $q_s = -K\nabla h_1$, where q_s is the specific discharge, K is the hydraulic conductivity, ∇ is the del operator, and h_1 is the head distribution. We used a constant K because the sediments used in flume experiments were essentially homogeneous. The seepage velocity or pore velocity, q_p, was calculated from the specific discharge using the porosity, θ, $q_p = \frac{q_s}{\theta}$. The interfacial boundary flux, $q_{\text{int}} = \hat{n} \cdot q_s$, was calculated based on the local value of the Darcy velocity and the unit normal to the surface, $\hat{n}$. Measurements of surface topography were fit with a discrete Fourier transform in order to create a differentiable function, which allowed us to easily calculate the normal vector at any point on the streambed surface.

[18] Hyporheic exchange flow paths and subsurface residence time distributions were determined from the subsurface flow field by particle tracking. To evaluate exchange, 1000 particles were distributed over the streambed surface at locations randomly selected from a probability distribution proportional to the boundary influx. Particle motion in the subsurface was deterministic, as it was calculated based solely on the calculated seepage velocity distribution. Dispersion was neglected because other studies have found this to have only a small effect on residence times for the homogeneous sediments and scale of topography included in this model [*Elliott and Brooks*, 1997a, 1997b; *Salehin et al.*, 2004]. Particles were tracked through the system using a constant distance step, D_{Step}, and a variable time step. The selection of D_{Step} is delicate as smaller values yield more accurate results, but also substantially increase the amount of time required to perform particle tracking. In each iteration, the local seepage velocity was calculated from a linear interpolation of the head distribution at each particle location, and each particle was then translated by the distance D_{Step} in the direction of the seepage velocity. The periodicity imposed on the model domain allowed us to track the fate of particles that reached the downstream boundary simply by reintroducing them into the domain at the corresponding location of the upstream boundary. The location of each particle was tracked relative to the streambed surface at every step in the particle-tracking routine. The subsurface residence time distribution was calculated simply by recording the amount of time that each tracked particle took to return to the surface water. The resulting residence time distribution was flux weighted because the particles were introduced to the subsurface in proportion to the boundary flux.

3. Model Testing and Application

[19] Two laboratory data sets are used here to illustrate the functionality of the approach and to explore patterns and rates of hyporheic exchange over the bed-form-to-reach scale. First, we simulate exchange with a regular series of essentially two-dimensional dunes in a laboratory flume. The topographic information for this case consists of finely spaced topographic data along the centerline of the channel. Modeling this 2-D case did not require a conformal mapping of the head boundary condition, but it did use the head calculation from the Fourier decomposition, interfacial flux calculation, and particle tracking procedure. This experiment also included observations of solute exchange with the bed, which we compare against the model simulations in order to evaluate the Fourier series exchange model for a spectrum of 2-D topography. Second, we simulate exchange in a naturally meandering channel generated in a relatively wide flume. No measurements of solute transport are available for this second data set, but it is included here because the highly detailed observations of 3-D stream topography allow us to investigate the interplay of exchange between bed forms and meanders.

3.1. Exchange With Dunes and Ripples

3.1.1. Experiment Setup

[20] A recirculating flume, which allowed for sediment transport, was used for this experiment. It was 12 m long, 26.5 cm wide, 25.4 cm deep. The flume contained high-purity silica sand (Ottawa 3.0) with a geometric mean diameter of 480 microns. The sand had a porosity of 0.33 and a hydraulic conductivity of 9 cm/min at an average bed depth was 10.5 cm. Bed topography was generated naturally by sediment transport under a uniform overlying flow 9.8 cm deep and having a mean velocity of ~25 cm/s. This led to the formation of a series of dunes and ripples that were nearly two-dimensional, generally spanning the width of the channel but with some irregularity in the shape resulting from the relatively narrow flume. After the bed topography was established, the stream discharge and slope were decreased until there was no bed sediment transport, and then the solute injection experiment was performed under steady uniform flow conditions. During the solute

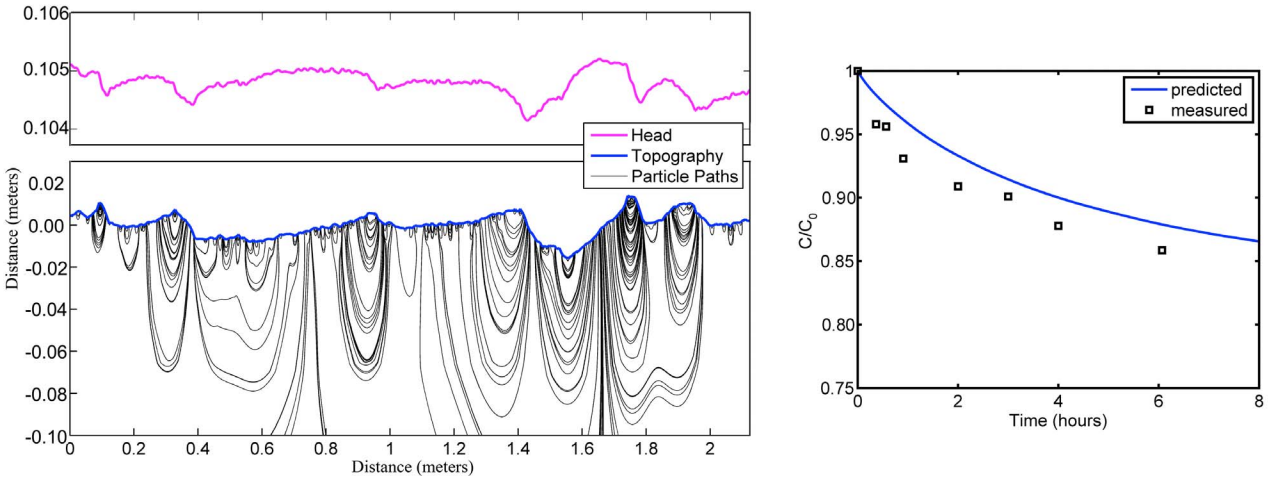

Figure 5. (left) Predicted head (magenta), observed streambed topography (blue), and simulated hyporheic exchange flow paths (black) for the two-dimensional case. (right) Predicted and measured normalized in-stream tracer concentrations for this case.

injection, the average stream depth was 9.8 cm, the mean velocity was 16.7 cm/s, and the slope was 0.00022. Lithium was used as the conservative tracer. A solution of lithium chloride was added to the flume to establish a uniform initial concentration of $C_0 = 38.9$ μM in the stream water. Surface-subsurface exchange caused the in-stream concentration to decrease over time owing to mixing (dilution) with tracer-free pore water. The primary solute transport is thus a time series of measurements of the in-stream lithium concentration, obtained by ICP-MS (Perkin-Elmer Elan 5000). The initial concentration is used to normalize all of the later solute measurements.

[21] The bed form topography was characterized using a laser profiler (Keyence LD-1101), which provided a series of high-resolution bed surface elevation measurements along the centerline of the flume. The laser profiling provides more detailed information on smaller-scale topographical features, like ripples, than can be obtained by visual or acoustic measurements, making this an excellent data set for model application and testing. This device was mounted on flume rails and driven by a stepper motor. Reflections due to the water surface were avoided by mounting the laser in a waterproof box with a glass bottom, which was lowered into the stream. Point elevation measurements were made every 9.1 mm and have a precision of ~10 μm. The topography data set consists of 588 evenly spaced points, which spanned a distance of 5.33 m.

3.1.2. Simulations and Results

[22] We used the model described in section 2 to predict pore water flow paths and solute exchange in this experiment. The subsurface model domain consisted of a 1762 × 83 × 17 grid. Particles were tracked through this system with a constant $D_{Step} = 10^{-5}$ m. The results were compared with the measured solute concentration data. The calculated boundary head over the two-dimensional topography and hyporheic exchange streamlines are shown in Figure 5 (left). These results clearly demonstrate the correspondence between topography and head, as well as the location of the maximum head upstream of the bed form crests. Calculated flow paths qualitatively match flow patterns commonly observed in dye tracer experiments in flumes [*Elliott and Brooks*, 1997b]. However, in contrast to previous models that use only a single representative scale of topography, the streamlines can be seen to reflect the multiple scales of topography found in this system.

[23] We used the approach of *Elliott and Brooks* [1997a, 1997b] to predict the change in in-stream concentration from the simulated boundary exchange flux and subsurface residence time distribution. This involved numerically solving the following convolution integral:

$$\frac{C(t)}{C_o} = 1 - \frac{\overline{q}}{d' C_0} \int_0^t \overline{R}(\tau) C(t-\tau) d\tau, \tag{8}$$

where overbars indicate spatial average over the streambed, $C(t)$ is the in-stream concentration, $\overline{q}$ is the spatially averaged interfacial flux, d' is the effective stream depth: the ratio between the total volume of stream water and the surface area of the sediment bed, $\overline{R}(t)$ is the flux-weighted cumulative residence time distribution, t is the time since the solute was added to the system, and τ is the time at which solute entered the subsurface. The predicted and observed time series of normalized in-stream tracer concentrations are presented in Figure 5 (right). The predicted concentrations match the shape of the curve and reproduce the measured values with an average error of 2.0% and a maximum error of 3.2%. The interfacial flux can be calculated directly from the initial slope of the C(t) curve, $\overline{q} = d'(\Delta C(t)/C_0 \Delta t)$. The observed interfacial flux was 5.07E-6 m/s, whereas the flux predicted by the model was 6.24E-6 m/s, corresponding to an error of 19%. These results show that the model provides a reasonable first-order approximation for hyporheic exchange under complex streambed topography.

3.2. Exchange With a Meandering Channel

3.2.1. Experimental Setup

[24] Our second test case was the slightly meandering stream shown in Figure 6. The channel was formed naturally by sediment transport in the tilting bed flume of the St.

Figure 6. Meandering channel in a tilting flume.

Anthony Falls Laboratory (SAFL), University of Minnesota. The flume, shown in Figure 6, was 14.6 m long, 0.9 m wide and 0.6 m deep. The upstream end of the flume had a 1.9 m long by 0.9 m wide head box, which provided smooth and uniform entry of water into the test section. The main channel test section included a 12 m long sediment bed. The water depth and discharge in the flume were controlled by a tailgate at the downstream end. Uniform flow was obtained by adjusting the slope and tailgate height to match the average energy grade line for the imposed discharge, bed sediments, and emergent bed morphology. The flume was continuously supplied with river water during the formation of the channel. All experiments were performed with Nelson Safety Grit sand (Nelson Quarry, Ontario, Canada) with d_{50} = 1.0 mm. The sediment had a relatively narrow size distribution, with 90% having a diameter finer than 3 mm, 30% finer than 0.8 mm and only 3% finer than 0.3 mm. The porosity, θ, of the sediment was measured and found to be 0.37. The hydraulic conductivity, K, was measured using a constant head permeameter and found to be 0.11 cm/s.

[25] The meandering channel was formed by cutting a straight trapezoidal channel of W = 35 cm, d = 4 cm in the sediment bed, with half of a meander bend included at the upstream end of the flume (following *Olsen* [2003]). Water was supplied at bank-full depth, a velocity of 50 cm/s, and channel slope (S_s) of 0.007. Flow around the initial meander bend led to the formation of a series of meanders. During this period of channel formation, sediments were supplied at the upstream end of the flume by a sediment feeder (Accurate, model 580–353600A). The meanders were allowed to grow until they approached the channel walls after approximately 4 h, at which point the slope and discharge were reduced until sediment transport ceased, leaving relict channel and bed form topography.

[26] The resulting meandering channel had four well-defined meander bends with an average wavelength of 2.20 m and average amplitude of 0.08 m. The topography of the meandering channel was measured with a sonar transit system mounted on a three-dimensional positioning instrument carriage that traversed the length of the flume. The bed profile was measured along 16 longitudinal transects evenly spaced across the channel width, with 136 regularly spaced elevation measurements along each transect. The average curvature of the stream was 0.43 m^{-1}, yielding an average radius of curvature of 2.3 m and a sinuosity of 1.01. The ratio of the radius of curvature to the stream width was thus 5.7. Variations in depth were relatively small and uniform within the meanders. Uniform streamflow through this meandering channel was observed to have an energy grade line slope of 0.0013, a mean depth of 3.8 cm, and a mean velocity of 16 cm/s.

[27] This channel morphology represents a case of incipient meandering. Much greater sinuosity can be found in nature, but this laboratory-generated meandering channel is a useful test case for initial application of the 3-D exchange model because the stream morphology was characterized in detail, the underlying sediments were homogeneous, and the hydraulic conductivity, porosity, and streamflow conditions were known precisely. Unfortunately no solute injection results are available for this case, but the high-quality observations of channel topography, sediment properties, and streamflow still make this a useful data set.

3.2.2. Simulations and Results

[28] For the three-dimensional simulation, we modeled the entire sediment bed under and around the four meanders, out to the channel walls. The side and bottom planes were defined as no-flow boundaries, corresponding to the sidewalls and bottom of the flume, respectively. The top surface of the domain includes the meandering stream channel and extends to the flume walls. Head values at the stream-subsurface interface were assigned according to the Fourier model described in section 3.2.1. The free surface outside of the stream was calculated using a separate MODFLOW simulation on an unconfined two-dimensional grid, based on the calculated head distribution within the stream channel and no-flow boundaries at the channel walls. The resulting head surface was then used as the top boundary outside the stream channel in the 3-D MODFLOW simulation. Note that the heads inside and outside the stream channel match exactly at the limit of the stream banks even when the velocity head is included within the stream because $V \rightarrow 0$ along the line of contact.

[29] We created a grid 17 layers deep with a higher density of layers near the surface in order to better resolve shallow hyporheic exchange flow paths. The top layer was 0.0002 m thick, each subsequent layer increased in thickness by a factor of 1.5, and a thin bottom layer (0.002 m) was included to improve the simulation of flow paths that approached this no-flow boundary. The grid was composed of 676 × 96 × 17 cells and D_{Step} = 0.001 m. We confirmed that this value of D_{Step} was sufficiently small so as not to affect the results. We represented the banks of the meandering channel using a 272-point polygon. The topography data set consists of an 136 × 16 orthogonal grid. The stream channel boundaries were defined from these measured values as described in section 2.2. The limited resolution of the topographic measurements caused the initial estimates of the stream bank to be rough, so we smoothed the banks using a moving average with a 26 cm window, thereby eliminating truly local edge anomalies.

[30] We ran multiple simulations of hyporheic exchange, including not only the full observed system complexity, but also simplified representations of the system. We used smoothed and idealized representations of the channel topography to evaluate how various scales of topography affect boundary fluxes and subsurface residence time distributions.

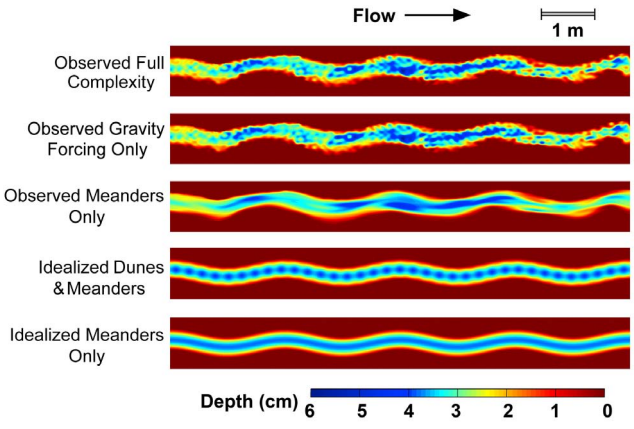

Figure 7. Topography and boundary head components used in each of the five simulation cases.

We also used reduced formulations of the boundary head distribution to show how gravitational and velocity head components interact to control patterns and rates of hyporheic exchange. The motivation for examining several cases with varying levels of detail is to determine how much complexity is required to capture the main effects when simulating hyporheic exchange processes.

[31] The topography and boundary head components used in each test case shown in Figure 7. Three cases were based on the observed, naturally formed channel topography. The observed full complexity case (OF) is our best estimate of the surface-subsurface exchange in the SAFL experiments, including the full topographic complexity and pore water flow induced by both gravitational and velocity head components. The observed gravity forcing only case (OG) includes the full topographic complexity, but only includes the gravitational head and mean velocity head of the stream, and does not add the velocity head variation associated with streamflow over bed forms. Comparison of the OF and OG cases allows us to evaluate the contribution of the velocity head fluctuations. The observed meanders only case (OM) is a filtered data set that includes only large-scale topography, and thus represents a smoothed version of the stream without bed forms (dunes and ripples). For this channel morphology, the cutoff between small and large topography required to satisfy the slope requirements of the gradually varied flow equations was $\lambda_c = 2W$, where W is the mean width of the stream. Thus case OM includes components of the observed topographic spectrum with longitudinal wavelengths $\lambda(\xi) > 2W$ (80 cm).

[32] The remaining two cases were idealized stream channels. The idealized meanders (IM) case was made up of a simple sinusoidal stream, where the centerline of the channel was a sine curve having the same mean amplitude and wavelength as the actual channel, 0.078 m and 2.2 m, respectively. This idealized geometry also had the same average width as the actual stream channel and a parabolic bottom with the same mean depth. In the idealized dunes and meanders case (ID), small-scale topography was superimposed on the meanders in the form of idealized bed forms, represented as an additional sinusoidal variation in the downstream direction. The bed form amplitude was scaled by the stream depth in order to insure that the maximum amplitude occurred in the center of the stream and the amplitude approached zero at the banks. The mean amplitude was chosen to be H/2 = 0.0018 m, based on $H = 2\sqrt{2}\,\sigma_H(\xi)$ for the topography observed in the naturally formed stream channel. The idealized bed forms had a constant wavelength $\lambda = 0.25$ m, yielding a regular series of features. We obtained this single representative bed form frequency for the idealized morphology by integrating the power spectrum observed in the meandering channel with respect to frequency and then selecting the frequency that divided the area under the power spectrum function in half. Additionally, two smaller wavelength values were used. The results from these cases were qualitatively similar to the case presented in this paper and are included in the supplementary materials.

[33] Figure 8a shows particle paths resulting from each case described in Figure 7. Here the effect of small topography is clearly shown through the larger number of shorter flow paths. Specifically, in the OF and ID cases, 83% and 76% of the flow paths are less than two meters, while the other cases have no more than 20% of their flow paths meeting this criterion. Most of these short flow paths are driven by velocity head perturbations over the channel topography and enter the subsurface on the upstream side of dunes or ripples. These shorter pathways are important because they contribute the bulk of the exchange flow through the uppermost region of the bed. Models that neglect small topography will miss numerous short flow paths, which together account for substantial delivery of water to the subsurface. Such shallow, rapid exchange is particularly important for stream ecology and biogeochemistry, as these flows are responsible for replenishing highly labile and reactive solutes in the sediments, and therefore control spatial distributions of oxygen and other compounds derived primarily from the overlying water column.

[34] The spatial distribution of interfacial flux for each case is shown in Figure 8b. Positive fluxes represent flow into the subsurface and the negative fluxes represent flow out of the subsurface. Dunes and ripples produced significantly greater boundary exchange flux than did meanders, as can be seen by the lack of the meander-associated alternating pattern of influx and efflux in the OF and the ID cases. In these cases, velocity head perturbations over bed forms dominated the overall hyporheic exchange flux. The other three simplified cases all show distinct patterns of hyporheic exchange due to meanders. The maximum influx due to meanders occurred on the outer edges of the upstream side of the meander.

[35] The average interfacial flux into the stream was 1.2E-5 m/s (1.1 m/d) for OF, 1.2E-7 m/s (1.0 E-2 m/d) for OG, 9.4E-8 m/s (8.2E-3 m/d) for OM, 1.5E-6 m/s (1.3 E-1 m/d) for ID, and 7.1E-8 m/s (6.2 E-3 m/d) for IM. The interfacial flux associated with the OF case was between 8 and 170 times greater than the other cases. The ID case has the next highest interfacial flux. The selection of shorter wavelengths for the ID case increases the interfacial flux. The fully natural complexity OF case had 130× more flux than the OM case, and the idealized ID case had 21× more flux than the IM case. The fact that the interfacial flux is so much greater for the OF and ID cases demonstrates that the complex natural fine-scale topography (dunes and ripples) contributes significantly to the magnitude of interfacial flux and thus plays an important role in hyporheic exchange. It is important to note, however, that our stream

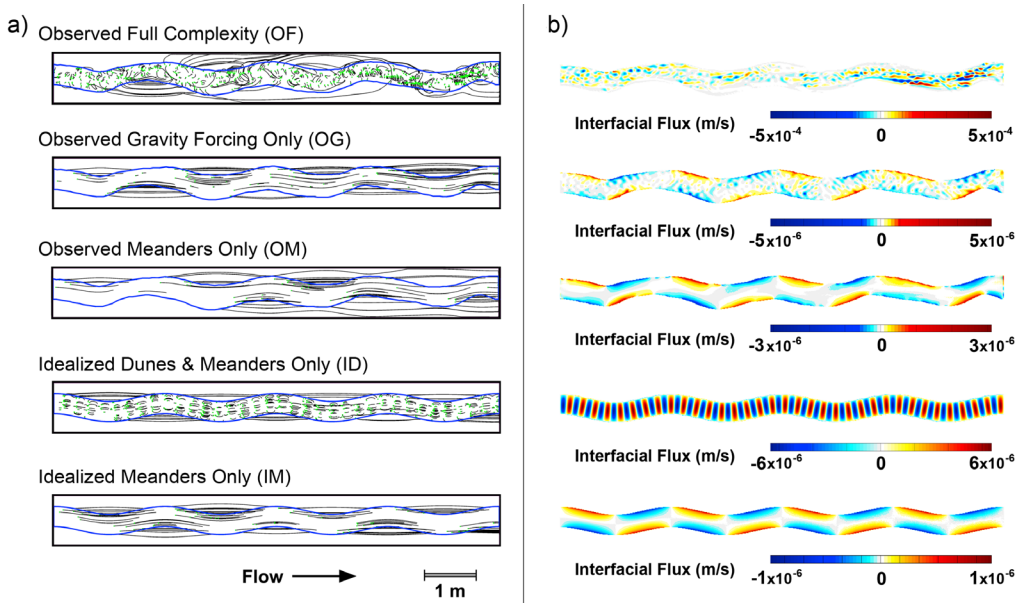

Figure 8. (a) Pore water flow paths and (b) distribution of interfacial flux associated with each case described in Figure 7. Case OF includes the full system complexity. The pattern of exchange is much more complex for this case than for any other case. Case OG includes the full topography but with only the gravitational head driving hyporheic flow. Cases OM and IM have smoothed topography and clearly exhibit alternating patterns of influx and efflux at the meander scale. OF and ID show that the head gradients associated with small topographical features overshadows the effect of meandering. The numerous short flow paths in OG, OF, and ID occur due to small topography. Note that the color scales in Figure 8b vary for each of the cases, largely because the interfacial flux associated with case OF is significantly greater than that of any other case.

had weak meanders and that larger meanders produce increased flux [*Boano et al.*, 2006; *Cardenas*, 2009b]. The amount of flux associated with the velocity head perturbation over small topography can be evaluated by comparing case OG with case OM and case OF. The flux in case OG was only 1.2× greater than case OM, while case OF was 106× greater than case OG, indicating that the velocity head perturbation is much more important than the morphology of the small topography itself. The velocity head is proportional to the square of the mean in-stream velocity, so this effect is highly dependent on the streamflow conditions.

[36] Cumulative residence time distributions also varied greatly when velocity head perturbations associated with the small topography were included, as shown in Figure 9. The cumulative residence time distribution is the fraction of exchanged water that remains in the subsurface, so it decreases monotonically as hyporheic flow reenters the surface water. The OF case had a much broader subsurface residence time distribution than any of the filtered or idealized cases, again illustrating that hyporheic exchange flows are induced by a wide range of spatial scales of stream topography. In general, the timescale of hyporheic exchange increases with the size of the topographic feature that induces it, so limited representations of the system, such as measuring only certain size classes of topography or characterizing topography only in terms of an average, are misleading because they only capture a narrow window of exchange timescales. The relative effects of the dune/ripple versus meander scales can be seen by comparing the results of the IM case, which included only a single scale of topography (large meanders), to the results of ID case, which included both large and small topography. Inclusion of the small topography caused the median residence time for ID to be approximately 20 times smaller than that for IM. The residence time distribution for the OM case, which was a smoothed version of the observed meanders containing only topographic features with $\lambda > 2W$, was much like the one for the IM case. This was expected given that this stream channel was formed under highly controlled conditions, and the meandering was highly constrained by the width of the flume. Natural meandering streams normally show a much greater diversity of planform morphology, which will lead to broader distributions of subsurface flow paths and residence times beyond the range of scales considered here. Nonetheless, even the limited spatial variability in the channel planform geometry here caused some lateral hyporheic flow paths to extend over multiple meanders. This led to case OM having a long tail in the cumulative residence time plot that was not present in the IM case. The OG case used the full observed topography without the local advective pumping associated with velocity head fluctuations. The residence time distribution for this case shows two distinct modes. The first and smaller decline in the cumulative plot corresponds to shorter pore water flow paths associated with dunes. The second decline coincides with the meander-scale flow paths. The meander-scale residence time is also found in both the OM and IM cases. The OG case also displays a long tail that is not present in the idealized cases, which further emphasizes that complex natural topographies produce extended subsurface storage.

[37] An alternative way to compare the fate of exchanged water between cases is to consider the cumulative residence

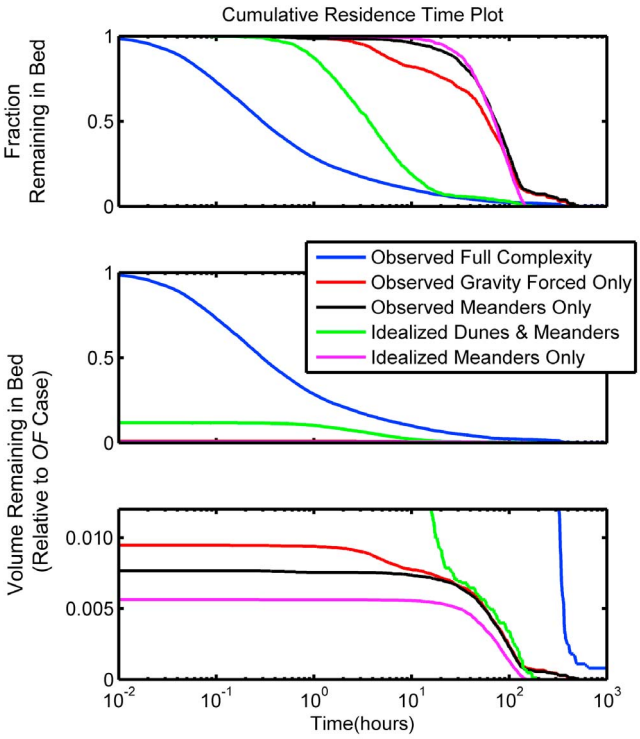

Figure 9. (top) Flux-weighted cumulative residence time distribution for each of the cases described in Figure 7. (middle) Volumetric residence time distribution for fraction of water remaining the bed normalized by volumetric exchange for the OF case. (bottom) Inset showing the same results shown in Figure 9 (middle) with vertical axis selected to illustrate the differences between cases OG, OM, and IM. Case OF has the lowest residence time but the largest exchanged volume remaining in the bed, illustrating the high rate of exchange associated with small topographical features.

time distribution based on the volume of exchanged fluid, rather than the residence time distribution normalized by the exchange flux. In Figure 9 (middle), we present the volumetric cumulative residence time distributions normalized by that the volume exchanged in case OF. From Figure 9 (top), it can be seen that the OF and ID cases had a smaller *fraction* of long residence times (greater than 10 h) than did the other three cases. However, the other cases did not actually produce a greater *volume* of exchanged water with long residence times. In fact, Figure 9 (middle) shows that cases OF and ID had so much more boundary exchange that they caused more water to remain in the subsurface for longer than 10 h than did the other three cases, despite the fact that they had a smaller fraction of the exchanged water remain for this duration. The large increase in boundary exchange for these cases is due to the inclusion of the velocity head perturbation associated with bed forms. This process produces higher local variability than does the gravitational head, thus producing greater head gradients over the bed surface and driving more pore water flow.

[38] The return flux in cases OG and ID occurred primarily over two distinct timescales, corresponding to the pore water flows induced by the small topography and the large topography. This appears as bimodality in the residence time distributions. In case ID, bed forms also showed a significant increase in short-duration exchange because of the bed form topography. However, both idealized cases (ID and IM) showed an earlier cutoff in the tails of their distributions relative to the cases with naturally formed topography because of their regular periodic morphology. The OF case had significantly more water remaining in the subsurface for long times than any of the other cases, demonstrating that interactions across the topographic spectrum substantially extend subsurface residence times. This occurs, for example, through the development of stagnation points because of the interaction of flows generated at different scales [*Wörman et al.*, 2007].

[39] Because the model explicitly constructs the residence time distribution from transport along individual hyporheic flow paths, it is also possible to examine the spatial distribution of residence time over the streambed surface. Figure 10 shows the amount of time that water entering the subsurface at different locations will spend in the subsurface. This result was obtained by means of particle tracking, with the particles released uniformly over the bed surface on a 1.3 cm by 1.0 cm grid. The simplified representations of topography yield not only regular patterns of exchange, but also a limited window of exchange timescales. The naturally formed meanders have patterns of exchange similar to the idealized case, but with a broader spectrum of residence times. The superposition of bed forms on meanders affects the length of time water spends in the subsurface. Small topography dominates patterns of exchange toward the center of the stream, while meanders have a larger effect on the residence time of water that enters the subsurface toward the edges the stream channel. Water that has a long subsurface residence time tends to consistently enter the subsurface at specific locations relative to topography for all of the cases. The flow paths with the longest residence times start just downstream of the apex of the meanders. Much of the water that enters the subsurface

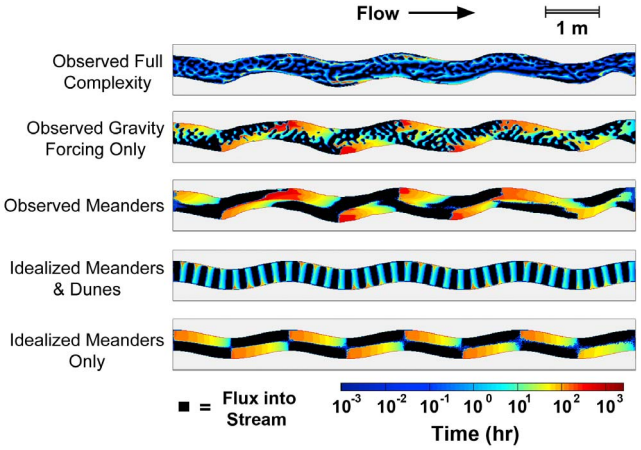

Figure 10. Spatial distribution of residence time for water exchanged at different locations on the streambed. These results were obtained by determining the travel time along hyporheic exchange flow paths originating at each point on the bed surface. Black areas correspond to regions of negative interfacial flux (flow out of the subsurface into the stream).

at these locations travels an entire meander length before reentering the stream.

4. Discussion and Conclusions

[40] We presented here a novel three-dimensional model for surface-subsurface interactions in low-gradient natural streams with gradually varied flow over different scales of channel morphology. We employed a spectral (Fourier series) approach to represent the complexity of the channel topography. We modeled the head distribution over the stream channel boundary by including the reach-scale head gradient plus an approximate quasi-three-dimensional solution for the local variation of velocity head over bed forms. These simplifying assumptions were needed to provide a tractable, efficient, and reasonably correct subsurface flow model based on the types of data that are typically available for investigations of solute transport in rivers. The aim of this work was not to simulate the stream and subsurface flow in perfect detail, but rather to capture the essence of multiscale hyporheic exchange resulting from both stream channel planform morphology and bed surface roughness. The primary advantage of this approach, in comparison to previous models, is that it predicts three-dimensional patterns of exchange resulting from multiple scales of fluvial topography spanning the range of ripples, dunes, alternate bars, and meanders. When applied to a centerline bed profile over a dune-ripple field in a laboratory flume, the maximum error between the model predictions and the observed stream concentration was 3.2%. These results indicate that this model provides a suitable first-order approximation of the boundary pressure distribution and pore water flow paths under dunes and ripples. Clearly this approximation does not capture the full three-dimensional flow-boundary interactions in detail, as computational fluid dynamics models do, but the approximate model is useful to investigate the role of local flow-boundary interactions in rates and patterns of hyporheic exchange over a wide range of spatial scales. The model assumptions are expected to be reasonable for low-gradient systems, where flow is fairly regular and uniform, but not for streams that have high slopes, significant non-uniformities, or transverse flow components relative to the local orientation of the channel.

[41] Application of the model to the case of a naturally formed, weakly meandering stream in a laboratory flume revealed the complexity of multiscale, three-dimensional hyporheic exchange. Regions of high flux were associated with both large- and small-scale features. The corresponding hyporheic exchange flow paths ranged from short paths under ripples to much longer paths spanning multiple meanders. Comparison of the exchange between the full observed complexity of the meandering channel and smoothed morphology shows that the bed-form-induced pumping process, resulting from local perturbations in the velocity head over small-scale topographical features such as ripples and dunes, plays a dominant role in driving interfacial flux (Figure 8a) and in controlling pore water flow paths (Figure 8b) and short-term components of the subsurface residence time distribution (Figure 9). Other researchers have suggested this to be the case [e.g., *Wörman et al.*, 2007; *Boano et al.*, 2009], but the present study is the first to confirm the dominance of small-scale features in meandering streams using a unified, multiscale modeling framework.

[42] The model simulations also show that there are complex interactions in exchange induced at various scales, so that simplifying the system to a small set of representative features greatly affects the prediction of interfacial fluxes and residence time distributions (Figure 9). The complex nature of the interactions between scales of topography deserves particular attention, as it leads to important implications for estimating exchange in natural systems. The complexity of interactions across scales means that the system cannot be easily decomposed, and scale limitations associated with both spatial resolution and domain size should be considered so as not to neglect relevant features. This is a reflection of the fractal nature of both fluvial topography and surface-groundwater interactions. When it is necessary to separate a defined subset of scales, such as a river reach, then it is extremely important to impose the correct boundary conditions on the subdomain, as the interactions due to features larger than the study reach are very likely to impact exchange within the reach. This suggestion is consistent with the broader findings of *Wörman et al.* [2007] and *Cardenas* [2008] for exchange associated with multiple scales of topography in different types of hydrogeologic systems, but here we provide compelling evidence based on our use of the new model to integrate interfacial flux and hyporheic exchange over naturally formed multiscale features typically found in lowland rivers (meanders and bed forms). This finding does not bode well for methods that attempt to model net exchange by linear summation or averaging of processes occurring at many individual scales, as that approach neglects the interactions between scales that appear to be highly prevalent in river systems and important in controlling patterns and rates of hyporheic exchange.

[43] It may still be possible to find a more direct method for simulating multiscale exchange, but this will be challenging. More accurate models of the in-stream velocity field and pore water velocity field generally cannot be applied over the range of scales considered here, especially when the coupling of fluid flow across the sediment-water interface is considered. Further, more advanced models require much more detailed data sets on channel morphology, in-stream velocity distributions, subsurface stratigraphy and heterogeneity, and surrounding groundwater flow conditions. That type of effort is feasible at the current time, but is extremely difficult and expensive, and thus is unlikely to be used in most field applications. A useful direction for immediate progress on this problem is to further refine approximate multiscale 3-D models similar to the one that we employ here in order to develop verified, generally applicable tools for assessment of hyporheic exchange in all of the major types of streams and rivers, following a classification scheme such as the ones recently promulgated by *Montgomery and Buffington* [1997] and G. Parker (*1D Sediment Transport Morphodynamics with Applications to Rivers and Turbidity Currents*, electronic book, 2004).

[44] The extension of the model to natural streams having different morphologies and flow conditions is a natural direction for future work. For field application, the method presented here would need to be extended to additional scales of morphology and adapted to include more complex forcing from groundwater, necessitating careful attention to subsurface boundary conditions. An important limitation here was that the size of the flume restricted the channel morphology to be only weakly meandering, and also greatly

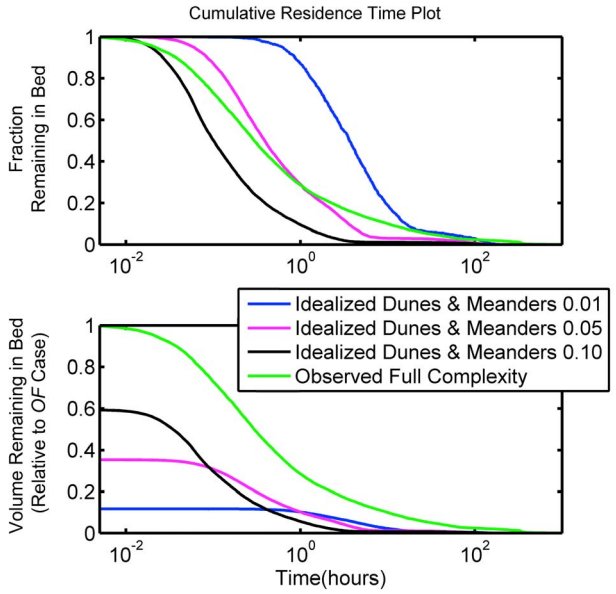

Figure A1. (top) Flux-weighted cumulative residence time distribution for three idealized dunes and meanders cases and the observed full complexity case. The ratio between twice the amplitude and the wavelengths of the dunes used in the ID cases was varied from the original 0.01 to 0.05 and 0.10. The amplitude was held constant, while the wavelengths were adjusted. All three of these ideal cases had steeper cumulative residence time plots than did the OF case. (bottom) Volumetric residence time distribution for fraction of water remaining the bed normalized by volumetric exchange for the OF case. ID 0.10 came the closest to matching case OF, but the flux is still too small and the shape is not correct. An even larger ratio would have yielded even smaller residence times, which would have increased the discrepancy seen in Figure A1 (top).

restricted the lateral extent of the meander-induced hyporheic flow paths. Thus, the size of the flume placed a sharp cutoff on the maximum scale of fluvial topography and also on the maximum scale of subsurface flow paths and residence times. The basic behavior found here is expected to extend across the entire topographic spectrum found in rivers, but will be subject to natural scale cutoffs associated with various types of channel formation processes [*Jerolmack et al.*, 2004; *Nikora et al.*, 1997] and the underlying hydrogeologic structure [*Marklund and Wörman*, 2010; *Salehin et al.*, 2004; *Packman et al.*, 2006; *Cardenas et al.*, 2004; *Sawyer and Cardenas*, 2009]. Larger-scale groundwater flow patterns are expected to influence rates and patterns of hyporheic exchange [*Wörman et al.*, 2007; *Cardenas*, 2008], so the model boundary conditions need to include the groundwater flow field surrounding the stream of interest.

[45] Current investigations of solute transport in rivers, particularly investigations focused on stream ecology and biogeochemistry, typically do not obtain regular, high-density measurements of channel morphology, essential hydrogeological properties such as permeability, or any information on groundwater levels outside the stream channel. It is important to realize that the ability to resolve multiple scales of hyporheic exchange depends directly on the effort put into characterizing system morphology, sediment properties, and overall surface and groundwater flow conditions. Further, the occurrence of strong, complex interactions across scales also implies that even local scale exchange will be highly influenced by processes occurring at the scale of the stream channel bars and meanders or even the regional groundwater flow field. Thus, valid quantitative predictions of surface-subsurface solute transport and effects on related biogeochemical processes (rates of oxygen consumption and cycling of nutrients and carbon, and fate of contaminants) are likely to be much improved with additional effort in characterizing channel geometry and flow variability, hydraulic conductitivity, and interactions with groundwater surrounding the stream.

Appendix A

[46] The ID case described in the primary text had a bed form height:wavelength ratio of 0.01. This aspect ratio was selected based on the channel morphology observed in the SAFL experiments, but is lower than commonly found in the field. In Figure A1 we present results from two additional ID cases with larger bed form aspect ratios. The dune height was held constant and the wavelength was shortened to produce aspect ratios of 0.05 and 0.10. The new cases had average interfacial fluxes of 4.4E-6 m/s (3.8 E-1 m/d) for $H/\lambda = 0.05$ and 7.3E-6 m/s (6.3 E-1 m/d) for the $H/\lambda = 0.1$ case as compared to the original ID case with $H/\lambda = 0.01$, which had 1.5E-6 m/s (1.3 E-1 m/d). Flux increases here with aspect ratio because the boundary head perturbation associated with bed forms occurs more frequently when the wavelength is shorter, while the amplitude of the head perturbation is constant because the bed form height was fixed. The largest flux, observed with the greatest aspect ratio and smallest wavelength, is still just 60% of that found in the OF case presented in the main text. An even shorter wavelength would yield the same fluxas the OF case, but it would also have even shorter residence times and would thus not truly match the distribution of residence times found in the OF case. These results support our conclusion that small (bed form) topography typically produces much more hyporheic exchange than large (planform) topography, but that interactions across scales substantially widen residence time distributions.

[47] **Acknowledgments.** The authors gratefully acknowledge financial support for this work from U.S. National Science Foundation grants EAR-0408744 and EAR-0810270 and a facilities access grant provided by the STC program of the NSF via the National Center for Earth-Surface Dynamics under agreement EAR-0120914. We thank Jeff Marr and Ben Erickson for their assistance in setting up and executing the experiments.

References

Bencala, K. E., and R. A. Walters (1983), Simulation of solute transport in a mountain pool-and-riffle stream: A transient storage model, *Water Resour. Res.*, *19*(3), 718–724, doi:10.1029/WR019i003p00718.

Benner, S. G., et al. (1995), Metal behavior during surface-groundwater interaction, Silver Bow Creek, Montana, *Environ. Sci. Technol.*, *29*(7), 1789–1795, doi:10.1021/es00007a015.

Boano, F., C. Camporeale, R. Revelli, and L. Ridolfi (2006), Sinuosity-driven hyporheic exchange in meandering rivers, *Geophys. Res. Lett.*, *33*, L18406, doi:10.1029/2006GL027630.

Boano, F., et al. (2009), Quantifying the impact of groundwater discharge on the surface-subsurface exchange, *Hydrol. Processes*, *23*(15), 2108–2116, doi:10.1002/hyp.7278.

Buffington, J., and D. Tonina (2009), Hyporheic exchange in mountain rivers, part II: Effects of channel morphology on mechanics, scales, and rates of exchange, *Geogr. Compass*, *3*(3), 1038–1062, doi:10.1111/j.1749-8198.2009.00225.x.

Cardenas, M. B. (2008), Surface water-groundwater interface geomorphology leads to scaling of residence times, *Geophys. Res. Lett.*, *35*, L08402, doi:10.1029/2008GL033753.

Cardenas, M. B. (2009a), Stream-aquifer interactions and hyporheic exchange in gaining and losing sinuous streams, *Water Resour. Res.*, *45*, W06429, doi:10.1029/2008WR007651.

Cardenas, M. B. (2009b), A model for lateral hyporheic flow based on valley slope and channel sinuosity, *Water Resour. Res.*, *45*, W01501, doi:10.1029/2008WR007442.

Cardenas, M. B., and J. L. Wilson (2007), Dunes, turbulent eddies, and interfacial exchange with permeable sediments, *Water Resour. Res.*, *43*, W08412, doi:10.1029/2006WR005787.

Cardenas, M. B., J. L. Wilson, and V. A. Zlotnik (2004), Impact of heterogeneity, bed forms, and stream curvature on subchannel hyporheic exchange, *Water Resour. Res.*, *40*, W08307, doi:10.1029/2004WR003008.

Cardenas, M. B., et al. (2008), Residence time of bedform-driven hyporheic exchange, *Adv. Water Resour.*, *31*(10), 1382–1386, doi:10.1016/j.advwatres.2008.07.006.

Chaudhry, M. H. (1993), *Open Channel Flow*, Prentice-Hall, Englewood Cliffs, N. J.

Driscoll, T. A. (1996), Algorithm 756: A MATLAB toolbox for Schwarz-Christoffel mapping, *Trans. Math. Software*, *22*(2), 168–186, doi:10.1145/229473.229475.

Elliott, A. H., and N. H. Brooks (1997a), Transfer of nonsorbing solutes to a streambed with bed forms: Theory, *Water Resour. Res.*, *33*(1), 123–136, doi:10.1029/96WR02784.

Elliott, A. H., and N. H. Brooks (1997b), Transfer of nonsorbing solutes to a streambed with bed forms: Laboratory experiments, *Water Resour. Res.*, *33*(1), 137–151, doi:10.1029/96WR02783.

Fehlman, H. M. (1985), Resistance components and velocity distributions of open channel flows over bedforms, M.S. thesis, Colo. State Univ., Fort Collins, Colo.

Fink, K., and J. Mathews (1999), *Numerical Methods Using MATLAB*, Prentice-Hall, Englewood Cliffs, N. J.

Fuller, C. C., and J. W. Harvey (2000), Reactive uptake of trace metals in the hyporheic zone of a mining-contaminated stream, Pinal Creek, Arizona, *Environ. Sci. Technol.*, *34*(7), 1150–1155, doi:10.1021/es990714d.

Harbaugh, A. W., et al. (2000), MODFLOW-2000, the US Geological Survey modular ground-water model: User guide to modularization concepts and the ground-water flow process, *U.S. Geol. Surv. Open File Rep.*, *00–92*, 1–121.

Harvey, J. W., and K. E. Bencala (1993), The effect of streambed topography on surface-subsurface water exchange in mountain catchments, *Water Resour. Res.*, *29*(1), 89–98, doi:10.1029/92WR01960.

Harvey, J. W., and B. J. Wagner (2000), Quantifying hydrologic interactions between streams and their subsurface hyporheic zones, in *Streams and Groundwaters*, edited by J. B. Jones and P. J. Mulholland, pp. 3–44, doi:10.1016/B978-012389845-6/50002-8, Academic, San Diego, Calif.

Jerolmack, D. J., and D. Mohrig (2005), A unified model for subaqueous bedform dynamics, *Water Resour. Res.*, *41*, W12421, doi:10.1029/2005WR004329.

Jerolmack, D. J., et al. (2004), A minimum time for the formation of Holden Northeast fan, Mars, *Geophys. Res. Lett.*, *31*, L21701, doi:10.1029/2004GL021326.

Jones, J. B., and P. J. Mulholland (Eds.) (2000), *Streams and Groundwaters*, Academic, San Diego, Calif.

Marklund, L., and A. Wörman (2010), The use of spectral analysis-based exact solutions to characterize topography-controlled groundwater flow, *Hydrogeol. J.*, in press.

McKnight, D. M., et al. (2001), Spectrofluorometric characterization of dissolved organic matter for indication of precursor organic material and aromaticity, *Limnol. Oceanogr.*, *46*(1), 38–48, doi:10.4319/lo.2001.46.1.0038.

Medina, M. A., et al. (2002), Surface water-ground water interactions and modeling applications, in *Environmental Modeling and Management: Theory, Practice and Future Directions*, edited by C. C. Chien et al., pp. 1–62, DuPont, Wilmington, Del.

Montgomery, D. R., and J. M. Buffington (1997), Channel-reach morphology in mountain drainage basins, *Geol. Soc. Am. Bull.*, *109*(5), 596–611, doi:10.1130/0016-7606(1997)109<0596:CRMIMD>2.3.CO;2.

Mulholland, P. J., et al. (1997), Evidence that hyporheic zones increase heterotrophic metabolism and phosphorus uptake in forest streams, *Limnol. Oceanogr.*, *42*(3), 443–451, doi:10.4319/lo.1997.42.3.0443.

Nikora, V. I., et al. (1997), Statistical sand wave dynamics in one-directional water flows, *J. Fluid Mech.*, *351*, 17–39, doi:10.1017/S0022112097006708.

O'Connor, B. L., and J. W. Harvey (2008), Scaling hyporheic exchange and its influence on biogeochemical reactions in aquatic ecosystems, *Water Resour. Res.*, *44*, W12423, doi:10.1029/2008WR007160.

Olsen, N. R. B. (2003), Three-dimensional CFD modeling of self-forming meandering channel, *J. Hydraul. Eng.*, *129*(5), 366–372, doi:10.1061/(ASCE)0733-9429(2003)129:5(366).

Packman, A. I., and K. E. Bencala (2000), Modeling methods in the study of surface-subsurface hydrologic interactions, in *Streams and Groundwaters*, edited by J. B. Jones and P. J. Mulholland, pp. 45–80, doi:10.1016/B978-012389845-6/50003-X, Academic, San Diego, Calif.

Packman, A. I., and N. H. Brooks (2001), Hyporheic exchange of solutes and colloids with moving bed forms, *Water Resour. Res.*, *37*(10), 2591–2605, doi:10.1029/2001WR000477.

Packman, A. I., et al. (2006), Development of layered sediment structure and its effects on pore water transport and hyporheic exchange, *Water Air Soil Pollut. Focus*, *6*(5–6), 433–442, doi:10.1007/s11267-006-9057-y.

Salehin, M., A. I. Packman, and M. Paradis (2004), Hyporheic exchange with heterogeneous streambeds: Laboratory experiments and modeling, *Water Resour. Res.*, *40*, W11504, doi:10.1029/2003WR002567.

Sawyer, A. H., and M. B. Cardenas (2009), Hyporheic flow and residence time distributions in heterogeneous cross-bedded sediment, *Water Resour. Res.*, *45*, W08406, doi:10.1029/2008WR007632.

Stream Solute Workshop (1990), Concepts and methods for assessing solute dynamics in stream ecosystems, *J. N. Am. Benthol. Soc.*, *9*(2), 95–119, doi:10.2307/1467445.

Thibodeaux, L. J., and J. D. Boyle (1987), Bedform-generated convective transport in bottom sediment, *Nature*, *325*(6102), 341–343, doi:10.1038/325341a0.

Tonina, D., and J. Buffington (2009), Hyporheic exchange in mountain rivers, part I: Mechanics and environmental effects, *Geogr. Compass*, *3*(3), 1063–1086, doi:10.1111/j.1749-8198.2009.00226.x.

Triska, F. J., et al. (1993), The role of water exchange between a stream channel and its hyporheic zone in nitrogen cycling at the terrestrial-aquatic interface, *Hydrobiologia*, *251*(1–3), 167–184, doi:10.1007/BF00007177.

Valett, H. M., et al. (1996), Parent lithology, surface-groundwater exchange, and nitrate retention in headwater streams, *Limnol. Oceanogr.*, *41*(2), 333–345, doi:10.4319/lo.1996.41.2.0333.

Williams, D. D., and H. B. N. Hynes (1974), The occurrence of benthos deep in the substratum of a stream, *Freshwater Biol.*, *4*(3), 233–256, doi:10.1111/j.1365-2427.1974.tb00094.x.

Winter, T. C., et al. (1998), Ground water and surface water: A single resource, *U.S. Geol. Surv. Circ.*, *1139*, 1–87.

Wörman, A., A. I. Packman, L. Marklund, J. W. Harvey, and S. H. Stone (2006), Exact three-dimensional spectral solution to surface-groundwater interactions with arbitrary surface topography, *Geophys. Res. Lett.*, *33*, L07402, doi:10.1029/2006GL025747.

Wörman, A., A. I. Packman, L. Marklund, J. W. Harvey, and S. H. Stone (2007), Fractal topography and subsurface water flows from fluvial bedforms to the continental shield, *Geophys. Res. Lett.*, *34*, L07402, doi:10.1029/2007GL029426.

Zarrati, A. R., et al. (2005), Mathematical modeling of meandering channels with a generalized depth averaged model, *J. Hydraul. Eng.*, *131*(6), 467–475, doi:10.1061/(ASCE)0733-9429(2005)131:6(467).

J. W. Harvey, U.S. Geological Survey, 430 National Center, Reston, VA 20192, USA. (jwharvey@usgs.gov)

A. I. Packman and S. H. Stonedahl, Department of Civil and Environmental Engineering, Northwestern University, 2145 Sheridan Rd., Evanston, IL 60208-3109, USA. (a-packman@northwestern.edu; susa@u.northwestern.edu)

M. Salehin, Institute of Water and Flood Management, Bangladesh University of Engineering and Technology, Dhaka 1000, Bangladesh. (mashfiqussalehin@iwfm.buet.ac.bd)

A. Wörman, Royal Institute of Technology, Teknikringen 76, SE-100 44 Stockholm, Sweden. (worman@kth.se)